Comparison of the Properties of $SnCl_3^-$ and $SnBr_3^-$ Complexes of Platinum(II)

John H. Nelson,*,† William L. Wilson,† Lewis W. Cary,† Nathaniel W. Alcock,‡ Howard J. Clase,§ Gouri S. Jas,|| Lori Ramsey-Tassin,|| and John W. Kenney, III||

Departments of Chemistry, University of Nevada, Reno, Nevada 89557, University of Warwick, Coventry CV47AL, England, and Memorial University of Newfoundland, St. John's, Newfoundland, and Department of Physical Sciences, Eastern New Mexico University, Portales, New Mexico 88130

Received June 25, 1995[⊗]

The complexes $M_3[Pt(SnX_3)_5]$ (M = Bu_4N^+, $PhCH_2PPh_3^+$; X = Cl, Br), *cis*-$M_2[PtX_2(SnX_3)_2]$ (M = Bu_4N^+, $PhCH_2PPh_3^+$, $CH_3PPh_3^+$, Pr_4N^+; X = Cl, Br), and $[PhCH_2PPh_3]_2[PtBr_3(SnBr_3)]$ have been prepared and characterized by ^{119}Sn and ^{195}Pt NMR, far-infrared, and electronic absorption and emission spectroscopies. In acetone solutions the $[Pt(SnX_3)_5]^{3-}$ ions retain their trigonal bipyramidal structures but are stereochemically nonrigid as evidenced by ^{119}Sn and ^{195}Pt NMR spectroscopy. For $[Pt(SnCl_3)_5]^{3-}$ spin correlation is preserved between 183 and 363 K establishing that the nonrigidity is due to intramolecular tin site exchange, probably via Berry pseudorotation. Whereas, $[Pt(SnCl_3)_5]^{3-}$ does not undergo loss of $SnCl_3^-$ or $SnCl_2$ to form either $[Pt(SnCl_3)_4]^{2-}$ or $[PtCl_2(SnCl_3)_2]^{2-}$, $[Pt(SnBr_3)_5]^{3-}$ is not stable in acetone solution in the absence of excess $SnBr_2$ and forms $[PtBr_2(SnBr_3)_2]^{2-}$ and $[PtBr_3(SnBr_3)]^{2-}$ by loss of $SnBr_2$. Similarly, $[PtCl_2(SnCl_3)_2]^{2-}$ is stable in acetone at ambient temperatures but disproportionates at elevated temperatures and $[PtBr_2(SnBr_3)_2]^{2-}$ loses $SnBr_2$ in acetone to form $[PtBr_3(SnBr_3)]^{2-}$. The crystal structures of methyltriphenylphosphonium *cis*-dibromobis(tribromostannyl)-platinate(II) and benzyltriphenylphosphonium tribromo(tribromostannyl)platinate(II) have been determined. Both compounds crystallize in the triclinic space group $P\bar{1}$ in unit cells with $a = 12.293(16)$ Å, $b = 12.868(6)$ Å, $c = 25.047(8)$ Å, $\alpha = 96.11(3)°$, $\beta = 91.06(3)°$, $\gamma = 116.53(3)°$, $\rho_{calc} = 2.30$ g cm^{-3}, $Z = 3$ and with $a = 11.046(7)$ Å, $b = 14.164(9)$ Å, $c = 22.549(10)$ Å, $\alpha = 89.44(4)°$, $\beta = 83.32(5)°$, $\gamma = 68.31(5)°$, $\rho_{calc} = 1.893$ g cm^{-3}, $Z = 2$, respectively. Least-squares refinements converged at $R = 0.057$ and 0.099 for 4048 and 4666 independent observed reflections with $I/\sigma(I) > 3.0$ and $I/\sigma(I) > 2.0$, respectively. For the former, the asymmetric unit contains 1.5 *cis*-$[PtBr_2(SnBr_3)_2]^{2-}$ ions, 0.5 of which is disordered in such a way as to be pseudocentrosymmetric. This disordering involves a half-occupied $PtBr_2$ unit appearing on either side of the center. Simultaneously, one bromine from each $SnBr_3$ ligand changes sides while the other two bromines appear in average positions with very small displacements between their positions. The Pt−Sn distance in $[PtBr_3(SnBr_3)]^{2-}$ (2.486(3) Å) is slightly shorter than that in *cis*-$[PtBr_2(SnBr_3)_2]^{2-}$ (2.4955(3) Å, average), and both are significantly longer than that previously found in *cis*-$[PtCl_2(SnCl_3)_2]^{2-}$ (2.3556 Å, average), which is not consistent with the relative magnitudes of the $^1J(^{195}Pt-^{119}Sn)$ coupling constants (28 487, 25 720, and 27 627 Hz, respectively). From our electronic absorption and emission studies of the Pt−SnX_3^- complexes, we conclude that (a) the low-energy transitions are d−d transitions analogous to those found in $[PtX_4]^{2-}$ systems, (b) the $SnCl_3^-$ ligand is a stronger σ donor than $SnBr_3^-$, (c) the triplet state from which the emission occurs is split by spin−orbit coupling into different spin−orbit states, (d) a forbidden spin−orbit state must lie at or near the bottom of the spin−orbit manifold, (e) the solid state crystal environment perturbs the platinum−tin halide electronic states, and (f) dispersion of the samples in solvents changes this perturbation, which can be rationalized in terms of an in-plane distortion of the square planar platinum coordination sphere.

Introduction

The interaction of platinum chlorides with stannous chloride has a long and interesting history.[1−3] As early as 1907, Wöhler[4] noted the intense colors of these solutions, which later served as a basis for the quantitative colorimetric determination of small amounts of platinum.[5] The exact nature of all the species responsible for the colors of these solutions still remains in some doubt, though we have shown by ^{119}Sn and ^{195}Pt NMR spectroscopy and X-ray crystallography that one yellow species is[6,7] *cis*-$[PtCl_2(SnCl_3)_2]^{2-}$ and a deep red species[6,8] is $[Pt(SnCl_3)_5]^{3-}$. Our efforts in this area were greatly aided by the seminal NMR investigations of Pidcock[9] and Pregosin.[10]

* Author to whom correspondence should be addressed.
† University of Nevada.
‡ University of Warwick.
§ Memorial University of Newfoundland.
|| Eastern New Mexico University.
⊗ Abstract published in *Advance ACS Abstracts,* February 1, 1996.

(1) Donaldson, J. D. *Prog. Inorg. Chem.* **1968**, *8*, 287.
(2) Karim, F. G.; Brackenburg, L. J.; Nel, I.; Koch, K. R.; Wyrley-Birch, J. M. *Polyhedron* **1987**, *6*, 71.
(3) Holt, M. S.; Wilson, W. L.; Nelson, J. H. *Chem. Rev.* **1989**, *89*, 11.
(4) Wöhler, L. *Chem.-Ztg.* **1907**, *31*, 938. See also: Wöhler, L.; Spengel, A. *Z. Chem. Ind. Kolloide* **1910**, *7*, 243. Shulka, S. K. *Ann. Chim. (Paris)* **1968**, *13*, 1383.
(5) (a) Wöbing, H. *Ber. Dtsch. Chem. Ges.* **1934**, *67B*, 773. (b) Ayres, G. H. *Anal. Chem.* **1953**, *25*, 1622. (c) Beamish, F. E.; McBride, W. A. E. *Anal. Chim. Acta* **1953**, *9*, 349. (d) Ayres, G. H.; Meyer, A. S. *Anal. Chem.* **1951**, *23*, 299. (e) Khattak, M. A.; Magee, R. J. *Talanta* **1965**, *12*, 733. (f) Pantani, F.; Piccardi, G. *Anal. Chim. Acta* **1960**, *22*, 231.
(6) Nelson, J. H.; Cooper, V.; Rudolph, R. W. *Inorg. Nucl. Chem. Lett.* **1980**, *16*, 263.
(7) Alcock, N. W.; Nelson, J. H. *J. Chem. Soc., Dalton Trans.* **1982**, 2415.
(8) Nelson, J. H.; Alcock, N. W. *Inorg. Chem.* **1982**, *21*, 1196.
(9) Pidcock, A. In *Catalytic Aspects of Metal Phosphine Complexes*; Alyea, E. C., Meek, D. W., Eds.; Advances in Chemistry Series 196; American Chemical Society: Washington, DC, 1982, p 1 and references therein.
(10) Ostoja-Starzewski, K. A.; Pregosin, P. S. In ref 9, p 22 and references therein.

0020-1669/96/1335-0883$12.00/0

Platinum(II)−tin(II) halide chemistry is emerging as an area of significance in structural and catalytic chemistry.[3] While numerous studies of the reactions of platinum(II) chloride complexes with $SnCl_2$ have been reported,[3] far fewer reports of analogous reactions of platinum(II) bromide complexes with $SnBr_2$ have appeared.[11−14] The optical properties of many platinum(II) complexes[15] including absorption, luminescence,[16−19] photoelectron,[20,21] and magnetic circular dichroism[22,23] spectra have been reported. Much attention in this area has been directed to the assignments of low-lying excited triplet and singlet states of these systems and the elucidation of the nature of spin−orbit coupling and vibronic interactions in these states. The ambient-temperature UV−visible absorption spectra of Pt(II)−SnX_3^--containing solutions have been reported.[5d,13,24] However, no detailed knowledge of the platinum complexes giving rise to the absorption bands was claimed and no band assignments were made. No electronic absorption or luminescence spectra have been measured for Pt(II)−SnX_3^- systems with well-defined chemical compositions. No temperature or time dependent luminescence measurements have been reported for any Pt(II)−Sn(II) halide system.

There are differences of opinion regarding the relative σ-donor and π-acceptor abilities of $SnCl_3^-$ and $SnBr_3^-$. The identical Fe−Sn bond distances in $(\eta^5\text{-}C_5H_5)Fe(CO)_2(SnX_3)$ (X = Cl, Br)[25] suggest that there is no difference. In contrast, the change in Mossbauer isomer shift and quadrupole splitting of the coordinated ligand as compared to those of the free ligand suggested[12] that $SnBr_3^-$ is both a stronger σ-donor and π-acceptor than $SnCl_3^-$.

In order to gain further insight, we have carried out a detailed study of the ^{119}Sn and ^{195}Pt NMR, far-infrared, and electronic absorption and emission spectral properties of analogous platinum(II)−$SnCl_3^-$ and −$SnBr_3^-$ complexes and report the results herein.

Experimental Section

Reagents and Physical Measurements. All chemicals were reagent grade and were used as received or synthesized as described below. Solvents were dried by standard procedures and stored over Linde 4 Å molecular sieves. All syntheses were conducted under a dry nitrogen atmosphere. $[Pr_4N][SnCl_3]$,[26] $[Bu_4N][SnBr_3]$,[26] $M_2[PtCl_2(SnCl_3)_2]$,[7] $M_3[Pt(SnCl_3)_5]$,[8] $M_2[PtBr_2(SnBr_3)_2]$,[13] and $M_3[Pt(SnBr_3)_5]$[13] were prepared by literature methods. Elemental analyses were performed by Galbraith Laboratories, Knoxville, TN. All new complexes gave satisfactory carbon, hydrogen, and halogen analyses. Infrared spectra were recorded on a Perkin-Elmer 1800 FT-IR instrument as Nujol mulls on polyethylene thin films. Melting points were obtained using a Mel-Temp melting point apparatus and are uncorrected. ^{119}Sn and ^{195}Pt NMR spectra were obtained at 186.36 and 107.43 MHz, respectively, on a Varian 500 Unity Plus spectrometer with chemical shifts relative to neat Me_4Sn and H_2PtCl_6 in D_2O/DCl, respectively. Positive values are downfield of the respective reference. A Hewlett-Packard (HP) 8452A diode array UV−visible spectrophotometer or a computer-interfaced Varian Cary 219 UV−visible spectrophotometer were used for electronic absorption measurements. All luminescence spectra were measured on a custom-built computer-controlled luminescence spectrophotometer. Samples were excited with a Xe/Hg arc lamp at 365 nm. Emitted light was analyzed by a Kratos GM 252 ($^1/_4$ m) monochromator operating with a red-sensitive Hamamatsu 7102 PMT. Luminescence spectra were intensity-corrected with respect to a standard lamp intensity profile. Low-temperature luminescence spectra were obtained by placing the sample in a liquid-nitrogen-filled quartz optical dewar for work at 77 K or in the sample holder of an Air Products Displex DE-202 closed-cycle liquid-helium refrigerator for variable-low-temperature spectroscopy in the 10 to 300 K range. Luminescence lifetimes were measured using an ∼10 ns pulsed PARC Model 2100 N_2 laser (337 nm) as the excitation source. The decay of the emitted light intensity of the sample after the laser pulse was monitored by a Hamamatsu R562 PMT connected to a HP54201A fast-digitizing storage oscilloscope whose time base was triggered by the initial laser pulse. A clean decay profile was obtained by averaging over 60−80 laser pulses. The luminescence lifetimes were extracted from the slopes of semilogarithmic linear least-squares plots of the emission intensity with respect to time.[27] The luminescence lifetime equipment was checked for calibration using samples of $[Ru(bipy)_3]Cl_2$ whose time-dependent luminescence behavior is well-known.

Synthesis. Benzyltriphenylphosphonium Tribromo(tribromostannyl)platinate(II), $[PhCH_2PPh_3]_2[PtBr_3(SnBr_3)]$. To a solution containing 0.59 g (1 mmol) of K_2PtBr_4[28] and 0.278 g (1 mmol) of $SnBr_2$ (Aldrich) in 25 mL of 6 M HBr, which had been stirred under N_2 for 1 h, was added a solution containing 0.87 g (2 mmol) of $[PhCH_2PPh_3]$-Br[29] in 25 mL of 95% ethanol. A yellow precipitate formed immediately. The mixture was stirred for an additional 1 h; the product was isolated by filtration, washed with 2 M HBr, 95% ethanol, and anhydrous diethyl ether and vacuum-dried to yield 0.29 g (82.1%) of yellow-brown solid, mp 164−165 °C. Recrystallization from acetone/$CHCl_3$/CCl_4 afforded deep red thin laths. Anal. Calcd for $C_{50}H_{44}$-Br_6P_2PtSn: C, 40.04; H, 2.93; Br, 31.97. Found: C, 39.76; H, 2.84; Br, 31.78.

X-ray Data Collection and Processing. Light red irregular-shaped blocks of **1** and deep red thin laths of **2** were obtained from acetone/hexane and acetone/$CHCl_3$/CCl_4, respectively. Crystal and diffraction data are given in Table 1. Experimental details are as follows for **1**, with those for **2** in parentheses when different. Data were collected with a Nicolet $P2_1$ (Siemens R3m) four-circle diffractometer in $\theta/2\theta$ mode using graphite-monochromated Mo Kα radiation. For **2**, the crystal was held at 200 K with an Oxford Cryosystems Cryostream Cooler.[30] Scan range was ±0.75 (0.5) (2θ) around the Kα_1−Kα_2 angles; scan speed was 2(3)−15° min^{-1}, depending upon the intensity of a 2 s prescan; backgrounds were measured at each end of the scan for one-fourth of the scan time. Three standard reflections were monitored every 200 reflections, and for **2** showed severe decay during data collection (30%), despite the reduced temperature (stable for **1**). The data were rescaled to correct for this. Unit cell dimensions and standard deviations were obtained by least-squares fit to 15 reflections ($20 < 2\theta < 22°$). Reflections were processed using profile analysis and were corrected for Lorentz, polarization, and absorption effects by the Gaussian method (the analytical method using ABSPSI).[31] There were no systematic reflection conditions; space group $P\bar{1}$ was assumed in both cases and shown to be successful by the satisfactory refinement.

(11) Adams, D. M.; Chandler, P. J. *Chem. Ind.* **1965**, 26.
(12) Antonov, P. G.; Kukushkin, Yu. N.; Mitronina, L. N.; Vasilev, L. N.; Sass, V. P. *Zh. Neorg. Khim.* **1979**, *24*, 1008.
(13) Antonov, P. G.; Kukushkin, Yu. N.; Shtrele, V. G.; Egorov, F. K.; Kostikov, Yu. P. *Zh. Obshch Khim.* **1982**, *52*, 2147.
(14) Koch, K. R. *Magn. Reson. Chem.* **1992**, *30*, 158.
(15) Chatt, J.; Gamlen, G. A.; Orgel, L. E. *J. Chem. Soc.* **1958**, 486.
(16) Webb, D. L.; Rossielo, L. A. *Inorg. Chem.* **1970**, *9*, 2622.
(17) Mason, W. R., III; Gray, H. B. *J. Am. Chem. Soc.* **1968**, *90*, 5721.
(18) Martin, D. S., Jr.; Lenhard, C. A. *Inorg. Chem.* **1964**, *3*, 1368.
(19) Martin, D. S., Jr.; Tucker, M. A.; Kassman, A. J. *Inorg. Chem.* **1965**, *4*, 1682.
(20) Bastusz, R.; Cahern, D.; Lester, J. E.; Rajaram, J. *Chem. Phys. Lett.* **1973**, *22*, 489.
(21) Cahern, D.; Lester, J. E. *Chem. Phys. Lett.* **1973**, *18*, 108.
(22) McCaffrey, A. J.; Schatz, P. N.; Stephens, P. J. *J. Am. Chem. Soc.* **1968**, *90*, 5730.
(23) Isci, H.; Mason, W. R. *Inorg. Chem.* **1984**, *23*, 1565.
(24) Meyer, A. S., Jr.; Ayers, G. H. *J. Am. Chem. Soc.* **1955**, *77*, 267.
(25) Bryan, R. F.; Greene, P. T.; Melson, G. A.; Stokely, P. F. *Chem. Commun.* **1969**, 722.
(26) Müller, U.; Mronga, N.; Schmacher, C.; Dehnicke, K. *Z. Naturforsch.* **1982**, *37B*, 1122.
(27) Demas, J. N. *Excited State Lifetime Measurements*; Academic Press: New York, 1983.
(28) Livingstone, S. E. *Synth. Inorg. Met.-Org. Chem.* **1971**, *1*, 1.
(29) Krubiner, A.; Oliveto, E. *J. Org. Chem.* **1966**, *31*, 24.
(30) Cosier, J.; Glazer, A. M. *J. Appl. Crystallogr.* **1986**, *19*, 105.
(31) Alcock, N. W.; Marks, P. J. *J. Appl. Crystallogr.* **1993**, *27*, 200.
(32) (a) Sheldrick, G. M. *SHELXTL User's Manual*; Nicolet: Madison, WI, 1983. (b) *SHELXTL PLUS User's Manual*; Nicolet: Madison, WI, 1986. (c) Sheldrick, G. M. *J. Appl. Crystallogr.*, in press.

Table 1. Crystallographic Data for $[CH_3PPh_3]_2[PtBr_2(SnBr_3)_2]$, **1**, and $[PhCH_2PPh_3]_2[PtBr_3(SnBr_3)]$, **2**

	1	**2**
formula	$C_{38}H_{36}Br_8P_2PtSn_2$	$C_{53}H_{44}Br_6Cl_9P_2PtSn$
fw	1626.11	1855.11
a (Å)	12.293(6)	11.046(7)
b (Å)	12.868(6)	14.164(9)
c (Å)	25.047(8)	22.549(10)
α (deg)	96.11(3)	89.44(4)
β (deg)	91.06(3)	83.32(5)
γ (deg)	116.53(3)	68.31(5)
V (Å^3)	3515(2)	3254(3)
space group	$P\bar{1}$	$P\bar{1}$
T (K)	290	200
Z	3	2
ρ_{calcd} (g cm^{-3})	2.30	1.893
λ (Å)	0.710 69	0.716 09
μ (mm^{-1})	11.51	6.667
$R(F)$ $[I > n\sigma(I)]^a$	0.057 ($n = 3$)	0.099 ($n = 2$)
$R_w{}^a$	0.056 (F)	0.362 (F^2), all data

^{a} $R(F) = \sum w(|F_o| - |F_c|)^2$. ^{b} $R_w = \sum w[(|F_o| - |F_c|)^2/\sum w|F_o|^2]^{1/2}$.

For **1**, heavy atoms were located by the Patterson interpretation section of SHELXTL,[32] and the light atoms were then found by *E* map expansion and successive Fourier syntheses. This revealed the two disordered pseudocentrosymmetric anions discussed below, with one complete anion in the asymmetric unit and a second one placed on a center of inversion. For **2**, structure solution proved difficult and, after extensive attempts using both direct methods and Patterson deconvolution, succeeded using Patterson search procedures (PATSEE within SHELXTL PLUS), based on a linked Br_3PtSn and a tetrahedral $SnBr_3$, with one free torsion angle (Pt−Sn, Pt−Br, and Sn−Br 2.5 Å, Pt−Sn−Br 97°). After further refinement, three disordered solvent molecules were also located, each modeled as rigid superimposed $CHCl_3$ and CCl_4, with the hydrogen of the former molecule essentially fixed but with refined slightly variable occupancies of the four chlorine positions. Anisotropic displacement parameters were used for all nonhydrogen atoms. Hydrogen atoms were given fixed isotropic displacement parameters, $U = 0.07$ (0.08) Å^2. Those defined by the molecular geometry were inserted at calculated positions and not refined; methyl groups were treated as rigid CH_3 units, with their initial orientation based on a staggered configuration. Final refinement was on F (F^2) by least-squares methods, including extinction parameters. Weighting schemes: **1**, $w = 1/(\sigma^2(F) + aF_o^2)$; **2**, $w = 1/(\sigma^2(F_o^2) + (aP)^2)$ where $P = (\max(0, F_o^2) + 2F_o^2)/3$; these were shown to be satisfactory by a weight analysis. The poor final R and high residual peaks in **2** are readily understandable in view of the serious decay and solvent disorder in this compound. Computing was with SHELXTL[32a] (SHELXTL PLUS[32b]) on a DEC Microvax-II (for **2**, final refinement by SHELXTL[32c] on an IBM PC system). Scattering factors in the analytical form and anomalous dispersion factors were taken from ref 33 and stored in the program. Final atomic coordinates are given in Tables 2 and 3 (supporting materials).

Results and Discussion

The complex $[PhCH_2PPh_3]_2[PtBr_3(SnBr_3)]$ (Figure 1) crystallizes as discrete ions with no unusual interionic contacts. Selected bond distances and angles are given in Tables 4 and 5. The $[PtBr_3(SnBr_3)]^{2-}$ ion is square planar, as the sum of the bond angles around platinum is 360.01°. The Pt−Br bond length for the bromide *trans* to $SnBr_3$ (2.478(4) Å) is significantly longer than the other two Pt−Br bond lengths (2.420(5) Å, average), and the latter are essentially the same as those found[34] in $[PtBr_4]^{2-}$ (2.418(10) Å, average). These results are in concert with the expectation[3] that the $SnBr_3^-$ ligand would have a large *trans* influence.[35,36] The Pt−Sn bond length (2.486(3) Å) is in the lower end of the range (2.34−2.80 Å)[3] of reported Pt−Sn bond lengths.

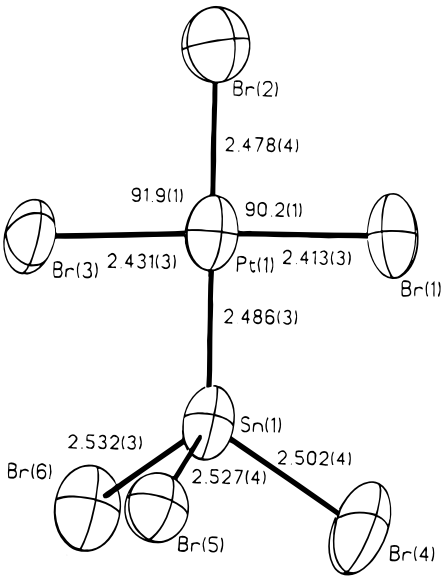

Figure 1. ORTEP drawing of the $[PtBr_3(SnBr_3)]^{2-}$ ion showing the atom-numbering scheme (50% probability ellipsoids).

Table 4. Comparative Bond Lengths (Å) for the Anions of *cis*-$[CH_3PPh_3]_2[PtBr_2(SnBr_3)_2]$, *cis*-$[PhCH_2PPh_3]_2[PtCl_2(SnCl_3)_2]$,[a] and $[PhCH_2PPh_3]_2[PtBr_3(SnBr_3)]$, with Standard Deviations in Parentheses

Disordered *cis*-$[PtX_2(SnX_3)_2]^{2-}$			
X = Br		X = Cl	
Pt(2)−Sn(3)	2.382(4)	Pt−Sn	2.3437(9)
Pt(2)−Sn(3a)	2.311(3)	Pt−Sn′	2.3675(7)
Pt(2)−Br(3)	2.435(2)	Pt−C1(1)	2.299(2)
Pt(2)−Br(4)	2.422(3)	Pt−Cl(2)	2.293(2)
Sn(3)−Br(31)	2.520(3)	Sn−Cl(3)	2.364(2)
Sn(3)−Br(32)	2.488(5)	Sn−Cl(4)	2.340(2)
Sn(3)−Br(4)	2.901(4)	Sn−Cl(2)	2.805(2)
Sn(3)−Br(3a)	2.883(4)	Sn−Cl(1′)	2.768(2)
Ordered *cis*-$[PtBr_2(SnBr_3)_2]^{2-}$			
Pt(1)−Sn(1)	2.503(2)	Pt(1)−Sn(2)	2.488(2)
Pt(1)−Br(1)	2.459(3)	Pt(1)−Br(2)	2.447(5)
Sn(1)−Br(11)	2.517(4)	Sn(1)−Br(12)	2.527(3)
Sn(1)−Br(13)	2.508(3)	Sn(2)−Br(21)	2.499(4)
Sn(2)−Br(22)	2.496(3)	Sn(2)−Br(23)	2.526(5)
$[PtBr_3(SnBr_3)]^{2-}$			
Pt(1)−Sn(1)	2.486(3)	Sn(1)−Br(4)	2.502(4)
Pt(1)−Br(1)	2.413(3)	Sn(1)−Br(5)	2.527(4)
Pt(1)−Br(2)	2.478(4)	Sn(1)−Br(6)	2.532(3)
Pt(1)−Br(3)	2.431(3)		

[a] Data from ref 7.

Both the $[PtBr_2(SnBr_3)_2]^{2-}$ and $[PtCl_2(SnCl_3)_2]^{2-}$ ions have an essentially square planar geometry and are isolated as the *cis* isomers. For $[CH_3PPh_3]_2[PtBr_2(SnBr_3)_2]$ the structure is disordered, containing an ordered *cis*-$[PtBr_2(SnBr_3)_2]^{2-}$ ion and a pair of disordered *cis*-$[PtBr_2(SnBr_3)_2]^{2-}$ ions with a pseudo center of symmetry. The disorder (illustrated in Figure 2) involves a half-occupied $PtBr_2$ unit appearing on either one or the other side of the center. Simultaneously, one Br on each Sn also changes sides, while the other two [Br(31) and Br(32)] appear in the crystal in averaged positions, but with only a small displacement between their two positions. The key to the disorder lies in Br(3) and Br(4). These are the *cis* bromines of

(33) Cromer, D. T.; Waber, J. I. *International Tables for X-Ray Crystallography*; Kynoch: Birmingham, England, 1974 (present distributor Kluwer Academic Publishers, Dordrecht, The Netherlands).
(34) Melanson, R.; Rochon, F. D.; Hubert, J. *Acta Crystallogr.* **1979**, *35B*, 736.
(35) Appleton, T. G.; Clark, H. C.; Manzer, L. E. *Coord. Chem. Rev.* **1973**, *10*, 335.
(36) Gofman, M. M.; Nefedov, V. I. *Inorg. Chim. Acta* **1978**, *28*, 1.

Table 5. Comparative Bond Angles (deg) for the Anions of *cis*-$[CH_3PPh_3]_2[PtBr_2(SnBr_3)_2]$, *cis*-$[PhCH_2PPh_3]_2[PtCl_2(SnCl_3)_2]$,[a] and $[PhCH_2PPh_3]_2[PtBr_3(SnBr_3)]$ with Standard Deviations in Parentheses

Ordered *cis*-$[PtBr_2(SnBr_3)_2]^{2-}$			
Sn(1)−Pt(1)−Sn(2)	96.1(1)	Sn(1)−Pt(1)−Br(1)	86.4(1)
Sn(2)−Pt(1)−Br(1)	174.4(1)	Sn(1)−Pt(1)−Br(2)	176.9(1)
Sn(2)−Pt(1)−Br(2)	87.0(1)	Br(1)−Pt(1)−Br(2)	90.6(1)
Pt(1)−Sn(1)−Br(1)	121.4(1)	Pt(1)−Sn(1)−Br(12)	123.5(1)
Br(11)−Sn(1)−Br(12)	94.1(1)	Pt(1)−Sn(1)−Br(13)	113.6(1)
Br(11)−Sn(1)−Br(13)	97.4(1)	Br(12)−Sn(1)−Br(13)	101.9(1)
Pt(1)−Sn(2)−Br(21)	119.2(1)	Pt(1)−Sn(2)−Br(22)	119.3(1)
Br(21)−Sn(2)−Br(22)	100.8(1)	Pt(1)−Sn(2)−Br(23)	118.7(1)
Br(21)−Sn(2)−Br(23)	96.7(2)	Br(22)−Sn(2)−Br(23)	97.6(1)
Disordered *cis*-$[PtBr_2(SnBr_3)_2]^{2-}$			
Sn(3)−Pt(2)−Sn(3a)	111.8(1)	Sn(3)−Pt(2)−Br(4)	74.3(1)
Br(3)−Pt(2)−Sn(3a)	74.7(1)	Br(3)−Pt(2)−Br(4)	99.2(1)
Pt(2)−Sn(3)−Br(31)	116.3(1)	Pt(2)−Sn(3)−Br(32)	125.3(1)
Pt(2)−Sn(3)−Br(3a)	122.8(1)	Br(4)−Sn(3)−Pt(2a)	121.5(1)
Br(31)−Sn(3)−Br(32)	102.1(2)	Sn(3)−Pt(2)−Br(3)	173.5(1)
Br(4)−Pt(2)−Sn(3a)	172.6(2)		
Disordered *cis*-$[PtCl_2(SnCl_3)_2]^{2-}$			
Sn−Pt−Sn′	111.48(3)	Sn−Pt−Cl(2)	74.44(6)
Sn′−Pt−Cl(1)	72.76(5)	Cl(1)−Pt−Cl(2)	101.32(8)
Pt−Sn−Cl(3)	119.58(7)	Pt−Sn−Cl(4)	124.47(5)
Pt−Sn−Cl(1′)	121.00(4)	Pt′−Sn−Cl(2)	120.47(4)
Cl(3)−Sn−Cl(4)	98.55(7)		
$[PtBr_3(SnBr_3)]^{2-}$			
Br(1)−Pt(1)−Br(2)	90.21(12)	Br(3)−Pt(1)−Br(2)	91.90(12)
Br(1)−Pt(1)−Sn(1)	89.64(10)	Br(3)−Pt(1)−Sn(1)	88.26(10)
Pt(1)−Sn(1)−Br(4)	123.50(13)	Pt(1)−Sn(1)−Br(5)	116.57(10)
Br(4)−Sn(1)−Br(5)	96.75(14)	Pt(1)−Sn(1)−Br(6)	117.40(11)
Br(4)−Sn(1)−Br(6)	98.38(14)	Br(5)−Sn(1)−Br(6)	99.66(12)

[a] Data from ref 7.

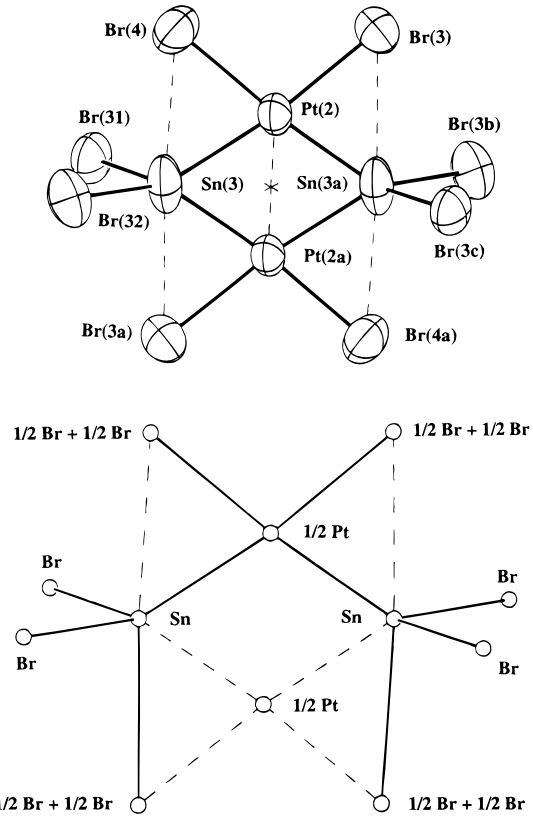

Figure 2. The disordered $[PtBr_2(SnBr_3)_2]^{2-}$ ion in $[CH_3PPh_3]_2[PtBr_2(SnBr_3)_2]$ showing the atomic numbering with an interpretation in terms of disordered atoms. The solid bonds show one orientation of the ion, while the dotted bonds exist in the alternative orientation.

the $PtBr_2$ unit, with half-occupancy. However, they are simultaneously the third bromine atom on each tin atom (also half-occupied). The result is that, irrespective of which alternative is present at any particular site in the crystal, the bromine contact envelope of the anion is virtually identical. We previously found[7] only pairs of disordered anions in the crystal structures of both *cis*-$[CH_3PPh_3]_2[PtCl_2(SnCl_3)_2]$ and *cis*-$[PhCH_2PPh_3]_2[PtCl_2(SnCl_3)_2]$. Comparative bond lengths and angles for the bromide and chloride complexes are given in Tables 4 and 5. These data are affected by the averaged positions of the halogen atoms. Consequently, only the Sn−Pt, Sn−Br(31), Sn−Br(32), Sn−Cl(3), and Sn−Cl(4) distances are likely to be reliable estimates, together with the Sn−Pt−Sn angles, and possibly the Br(31)−Sn(3)−Br(32) and Cl(3)−Sn−Cl(4) angles (as the alternative positions for these bromine and chlorine atoms are probably not much separated). The Pt−Sn distance in the bromide complex (2.4955(3) Å average for the ordered anion) (Figure 3) is significantly longer than that found[7] for *cis*-$[PtCl_2(SnCl_3)_2]^{2-}$ (2.3556(9) Å average). These Pt−Sn distances are shorter than those found[8] for the trigonal bipyramidal $[Pt(SnCl_3)_5]^{3-}$ ion (2.5530(7) Å, axial; 2.577(10) Å, equitorial). These comparative Pt−Sn distances suggest that the platinum−tin bond strengths decrease in the order *cis*-$[PtCl_2(SnCl_3)_2]^{2-}$ > $[PtBr_3(SnBr_3)]^{2-}$ > *cis*-$[PtBr_2(SnBr_3)_2]^{2-}$ > $[Pt(SnCl_3)_5]^{3-}$. Except for a reversal of the first two, the same order is found for the relative magnitudes of $^1J(^{195}Pt^{119}Sn)$ (*vide infra*). The Sn−Br distances (2.520 Å average for $[PtBr_3(SnBr_3)]^{2-}$, 2.504(5) Å average of Sn(3)−Br(31) and Sn(3)−Br(32) in *cis*-$[PtBr_2(SnBr_3)_2]^{2-}$) are shorter than those found[26] for $[PPh_4][SnBr_3]$ (2.624(1) Å average). Similarly, the Sn−Cl distances in the *cis*-$[PtCl_2(SnCl_3)_2]^{2-}$ ion[7] (2.353(2) Å, average) and the $[Pt(SnCl_3)_5]^{3-}$ ion[8] (2.363(6) Å, average) are shorter than those observed[26] for $[PPh_4][SnCl_3]$ (2.470(2) Å, average). Both $SnCl_3^-$ complexes contain $SnCl_3^-$ groups with similar Cl−Sn−Cl (∼95−100°) and Pt−Sn−Cl (∼117−122°) bond angles, which compare with Cl−Sn−Cl angles of ∼94−96° in $[PPh_4][SnCl_3]$. The Br−Sn−Br (∼94−119°) and Pt−Sn−Br (∼114−124°) angles show a greater variation, and the former compares with ∼93−98° in $[PPh_4][SnBr_3]$. These data suggest that the Sn−X bonds in the free SnX_3^- ions involve essentially only tin p orbitals with very little Sn s orbital participation. Upon coordination to platinum only a slight rehybridization of the SnX_3^- ion occurs such that the Pt−Sn bonds have considerable tin s character[37] and the Sn−X bonds have considerable tin p character, consistent with Bent's rules.[38] This is an ideal situation for Pt−Sn π-bonding.

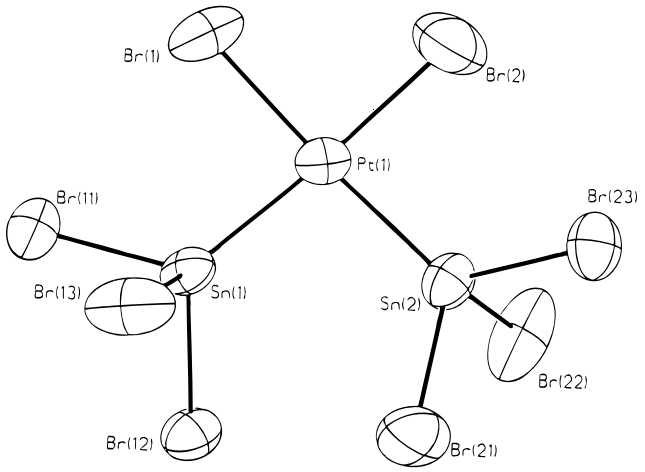

Figure 3. ORTEP drawing of the ordered $[PtBr_2(SnBr_3)2]^{2-}$ ion showing the atom numbering scheme (50% probability ellipsoids).

(37) Yamakawa, T.; Moriyama, H.; Shimoda, S.; Saito, Y. *Inorg. Chem.* **1987**, *26*, 3347.
(38) Bent, H. A. *Chem. Rev.* **1961**, *61*, 275.

Table 6. 186.36 MHz ^{119}Sn and 107.43 MHz ^{195}Pt NMR Data for Platinum(II) SnX_3^- (X = Cl, Br) Complexes[a]

complex ion	$\delta(^{119}Sn)$	$\delta^{195}Pt$	$^1J(^{195}Pt^{119}Sn)$	$^1J(^{195}Pt^{117}Sn)$	$^2J(^{117}Sn^{119}Sn)$
cis-$[PtCl_2(SnCl_3)_2]^{2-}$	−375.0	−4183	27 627	26 392	2936
$[Pt(SnCl_3)_5]^{3-}$	−130.7	−4701	16 046	15 310	6273
$[PtBr_3(SnBr_3)]^{2-}$	−600.8	−5469	28 487	27 174	
cis-$[PtBr_2(SnBr_3)_2]^{2-}$	−422.2	−4538	25 720	24 592	1675
$[Pt(SnBr_3)_5]^{3-}$	−238.0	−4272	14 939	14 249	6366

[a] In acetone/acetone-d_6 at 298 K. Chemical shifts in ppm relative to Me_4Sn (neat) and H_2PtCl_6 (in D_2O/DCl), respectively. Coupling constants in Hz. The uncertainties on chemical shifts and coupling constants are estimated to be ±5 ppm and ±20 Hz, respectively.

^{119}Sn and ^{195}Pt NMR Spectroscopy. The differences in the platinum−tin bond strengths for the complexes studied are clearly evidenced by the ^{119}Sn and ^{195}Pt NMR data (Table 6). Formation of $SnCl_3^-$ ($\delta(^{119}Sn) = -23.7$ ppm in $CDCl_3$) from $SnCl_2{\cdot}2H_2O$ ($\delta(^{119}Sn) = -186.8$ ppm in acetone-d_6) causes a marked deshielding of the ^{119}Sn resonance ($\Delta\delta = 163.1$ ppm).[39] Tin chemical shifts are notoriously solvent and temperature dependent,[10,39,40] so it is not surprising that these chemical shifts differ from those previously reported.[39] Formation of $SnBr_3^-$ ($\delta = -399$ ppm in $CDCl_3$) from $SnBr_2$ ($\delta = -58.7$ in acetone-d_6) causes a marked shielding of the ^{119}Sn resonance ($\Delta\delta = -340.3$ ppm), a chemical shift change that is about twice the magnitude of that found for the formation of $SnCl_3^-$ from $SnCl_2{\cdot}2H_2O$. Coordination of $SnCl_3^-$ to platinum(II) as in *cis*-$[PtCl_2(SnCl_3)_2]^{2-}$ ($\delta(^{119}Sn) = 375.0$ ppm) or $[Pt(SnCl_3)_5]^{3-}$ ($\delta(^{119}Sn) = -130.7$ ppm) causes a much greater shielding for the former than for the latter suggesting a greater platinum(II)−tin (II) π-back-donation in the former, consistent with the significantly shorter Pt−Sn bond distance in the *cis*-$[PtCl_2(SnCl_3)_2]^{2-}$ ion than in the $[Pt(SnCl_3)_5]^{3-}$ ion. Coordination of $SnBr_3^-$ to platinum(II) as in $[PtBr_3(SnBr_3)]^{2-}$ ($\delta(^{119}Sn) = -600.8$ ppm), *cis*-$[PtBr_2(SnBr_3)_2]^{2-}$ ($\delta(^{119}Sn) = -422.2$ ppm), or $[Pt(SnBr_3)_5]^{3-}$ ($\delta(^{119}Sn) = -238.0$ ppm)[14] is attendant with decreasing ^{119}Sn shielding with an increase in the number of $SnBr_3^-$ ions coordinated to platinum(II).

The relative intensities of the lines in the ^{119}Sn NMR spectra of the platinum(II)−SnX_3^- complexes may be used to identify the individual species.[3] This is nicely illustrated by the ^{119}Sn NMR spectra of the $[PtBr_3(SnBr_3)]^{2-}$, *cis*-$[PtBr_2(SnBr_3)_2]^{2-}$, and $[Pt(SnBr_3)_5]^{3-}$ species. For $[PtBr_3(SnBr_3)]^{2-}$ one would expect to observe a single ^{119}Sn resonance (relative intensity 1) flanked by satellites due to coupling to ^{195}Pt ($I = {}^1/_2$, 33.7% natural abundance) with relative intensities of 0.25 (Figure S-1, supporting materials). For *cis*- $[PtBr_2(SnBr_3)_2]^{2-}$, because ^{119}Sn ($I = {}^1/_2$, 8.58% natural abundance) and ^{117}Sn ($I = {}^1/_2$, 7.61% natural abundance) will both be present in *cis* positions, there will also be satellites due to ^{117}Sn−^{119}Sn coupling with relative intensities of 0.07. For $[Pt(SnBr_3)_5]^{3-}$ the ^{195}Pt satellites will still have a relative intensity of 0.25 but the ^{117}Sn satellites will now have a relative intensity of 0.16 (Figure 4).[14] The ^{195}Pt NMR spectrum (Figure 5) of $[PtBr_3(SnBr_3)]^{2-}$ should show a central resonance (relative intensity 1) flanked by ^{117}Sn and ^{119}Sn satellites of relative intensities 0.038 and 0.043, respectively. In this spectrum, the ratio of $^1J(^{119}Sn^{195}Pt)$ to $^1J(^{117}Sn^{195}Pt)$ should be equal to the ratio of the ^{119}Sn to ^{117}Sn gyromagnetic ratios, which is 1.046. The relative intensities of the ^{119}Sn and ^{117}Sn satellites in the ^{195}Pt NMR spectra of the *cis*-$[PtBr_2(SnBr_3)_2]^{2-}$ and $[Pt(SnBr_3)_5]^{3-}$ ions should be 0.10, 0.09 and 0.24, 0.21, respectively.

The observation of single ^{119}Sn resonances for the trigonal bipyramidal $[Pt(SnX_3)_5]^{3-}$ ions as seen in Figure 4 indicates

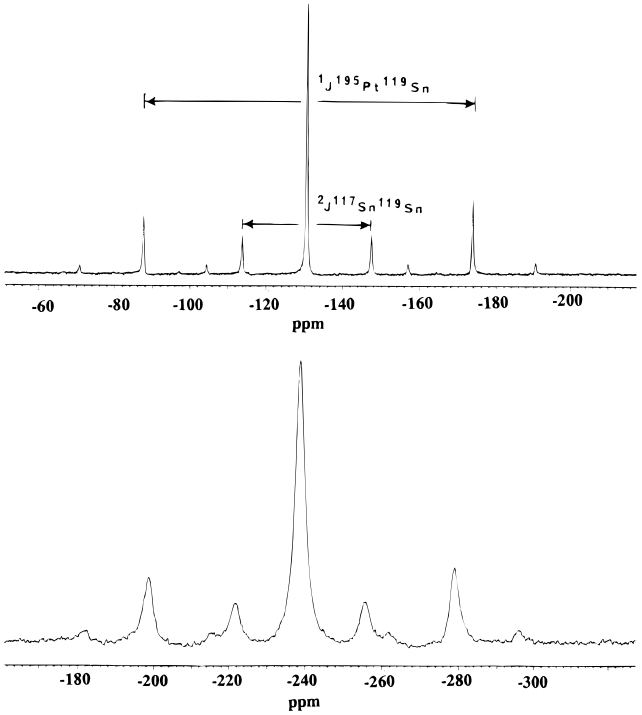

Figure 4. 186.36 MHz ^{119}Sn NMR spectra of $[PhCH_2PPh_3]_3[Pt(SnCl_3)_5]$ (upper) and $[PhCH_2PPh_3]_3[Pt(SnBr_3)_5]$ (lower) in acetone-d_6 at 298 K. For these two spectra the line widths at half-height ($\Delta\nu_{1/2}$) are 76 and 486 Hz, respectively.

the occurrence of a site-exchange process, and the maintenance of spin correlation suggests that this process is intramolecular. The greater line width for the $SnBr_3^-$ complex than for the $SnCl_3^-$ complex suggests that this process may be slower for the $SnBr_3^-$ complex. The platinum−tin coupling constants decrease in the order $[PtBr_3(SnBr_3)]^{2-}$ (28 487 Hz) > *cis*-$[PtCl_2(SnCl_3)_2]^{2-}$ (27 627 Hz) > *cis*-$[PtBr_2(SnBr_3)_2]^{2-}$ (25 720 Hz) > $[Pt(SnCl_3)_5]^{3-}$ (16 046 Hz) > $[Pt(SnBr_3)_5]^{3-}$ (14 939 Hz). This sequence is nearly the same as the sequence of the Pt−Sn bond lengths (where the data are available) and suggests that the Pt−Sn bond strength decreases in essentially this order.

It is now reasonably well established that the $SnCl_3^-$ group is a good π-acceptor,[3] and the X-ray and NMR data support this contention. The X-ray data for the *cis*-$[PtX_2(SnX_3)_2]^{2-}$ ions suggest that $SnCl_3^-$ is a better σ-donor and/or π-acceptor toward Pt(II) than is $SnBr_3^-$. For both *cis*-$[PtX_2(SnX_3)_2]^{2-}$ and $[Pt(SnX_3)_5]^{3-}$, the platinum−tin coupling constants are larger for the $SnCl_3^-$ complexes than for the $SnBr_3^-$ complexes, further supporting this contention.

Far-Infrared Spectroscopy. Coordination of SnX_3^- to platinum(II) removes electron density from the tin atom. This loss of electron density is compensated by π-bonding between tin and the halogen, thus shortening the tin−halogen bond and shielding the tin nucleus as previously noted. As a consequence, one would expect to observe ν(SnX) at higher energies for SnX_3^- complexes than for free SnX_3^- ions. This expectation is borne out by the far-infrared data (Table 7). It should be

(39) $\delta = -238$ for $SnCl_2{\cdot}n$THF in THF/C_6D_6, $\delta = 30.0$ for $SnCl_3^-$ in CH_2Cl_2/C_6D_6, and $\delta = -70.7$ for $SnBr_2{\cdot}n$THF in THF/C_6D_6 have been reported: Hani, R.; Geanangel, R. A. *Coord. Chem. Rev.* **1982**, *44*, 229.

(40) Smith, P. J.; Smith, L. *Inorg. Chim. Acta Rev.* **1973**, *7*, 11.

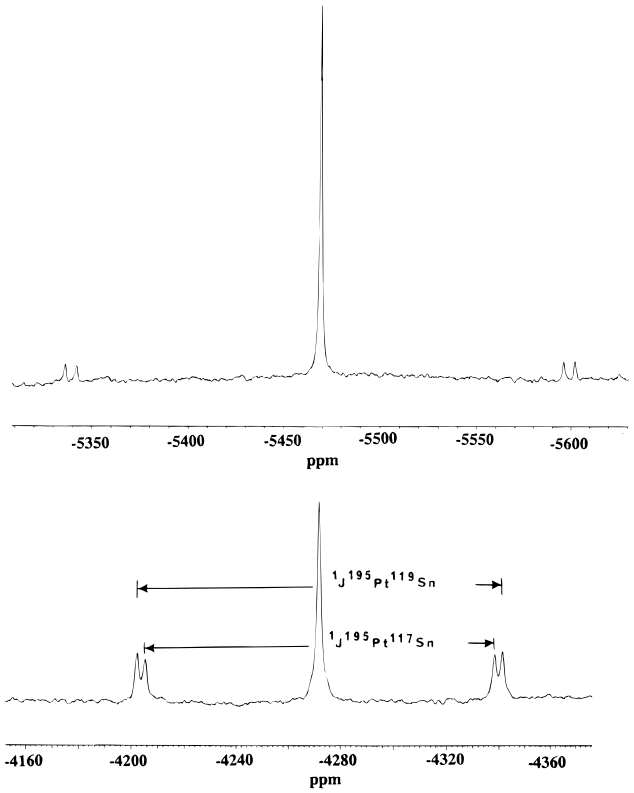

Figure 5. 107.43 MHz ^{195}Pt NMR spectra of $[PhCH_2PPh_3]_2[PtBr_3(SnBr_3)]$ (upper) and $[PhCH_2PPh_3]_3[Pt(SnBr_3)_5]$ (lower) in acetone-d_6 at 298 K.

noted, however, that irrespective of any reasonable bonding arguments, the shortening of SnX bonds on coordination of SnX_3^- would be expected to lead to higher ν(SnX). Coordination of $SnCl_3^-$ to platinum(II) as in *cis*-$[PtCl_2(SnCl_3)_2]^{2-}$ or $[Pt(SnCl_3)_5]^{3-}$ results in an increase in ν(SnCl) of about 84 cm^{-1}. Coordination of $SnBr_3^-$ to platinum(II) as in $[PtBr_3(SnBr_3)]^{2-}$, *cis*-$[PtBr_2(SnBr_3)_2]^{2-}$, or $[Pt(SnBr_3)_5]^{3-}$ results in an increase in ν(SnBr) by a smaller amount (16−64 cm^{-1}). This suggests that the Pt−Sn interaction in the Pt−$SnCl_3^-$ complexes is stronger than that in the Pt−$SnBr_3^-$ complexes which is consistent with the conclusions derived from the X-ray crystallographic and NMR data. It is interesting to note that the Pt−Sn vibrations occur at the same or slightly lower energy for the *cis*-$[PtCl_2(SnCl_3)_2]^{2-}$ ion compared to that for the $[Pt(SnCl_3)_5]^{3-}$ ion, even though the Pt−Sn bond is significantly shorter in the former. Similarly, the Pt−Sn vibrational energies increase slightly with an increase in the number of $SnBr_3^-$ ions coordinated to platinum(II). Both *cis*-$[PtX_2(SnX_3)_2]^{2-}$ ions exhibit two Pt−X vibrations in their far-infrared spectra consistent with the *cis* geometry of these complexes as determined by X-ray crystallography. There are no additional bands in their infrared spectra that are attributable to the disorder found in their crystal lattices.

Electronic Spectroscopy. The well-studied $[PtX_4]^{2-}$ complexes provide an insightful starting point for the interpretation of the electronic spectra of the Pt−SnX_3^- complexes.[16−19] Listed in Table 8 are UV−visible absorption band maxima with molar absorptivities and band maxima for the 77 K luminescence spectra of $[PtX_4]^{2-}$, *cis*-$[PtX_2(SnX_3)_2]^{2-}$, and $[Pt(SnX_3)_5]^{3-}$ where X = Cl and Br. Proposed transition assignments are also given in this table. Figures 6 and 7 show typical spectra.

Several trends are apparent in the spectral data of Table 8. Each absorption spectrum is composed of a number of bands whose molar absorptivities (ϵ) increase with increasing photon energy. In all cases, the absorption spectrum of the chloro complex is blue-shifted relative to the absorption spectrum of the corresponding bromo complex. A similar chloro *vs* bromo blue-shift pattern is observed in the luminescence spectra of these systems (Figures 6 and 7).

Mason and Gray[17] used ligand field theory to explain the electronic spectra of the $[PtCl_4]^{2-}$ and $[PtBr_4]^{2-}$ square planar systems. Their interpretations can be extended straightforwardly to provide a rationale for the general trends observed in the UV−visible absorption and luminescence spectra of the *cis* square planar and pentacoordinate Pt(II)−SnX_3^- complexes. SnX_3^- is a weak σ-donor analogous to the X^- ligand.[3] Just as Cl^- is higher in the spectrochemical series than Br^-, $SnCl_3^-$ is higher in the series than $SnBr_3^-$. The SnX_3^- ligand is also a π-acceptor ligand[3] whose Sn dπ orbitals are assumed to lie above the Pt(II) d orbitals in our adaptation of the Mason−Gray model to Pt(II)−SnX_3^- complexes. These empty Sn dπ dorbitals could serve as acceptors of Pt(II) electron density in metal-to-ligand charge transfer transitions in the UV region. Such transitions with the high molar absorptivities characteristic of charge transfer transitions are observed in the 37 000−45 000 cm^{-1} UV region of the absorption spectrum of the *cis* square planar $[NPr_4][PtCl_2(SnCl_3)_2]$ complex (Figure S-2, supporting materials).

Transition no. 1 for the *cis*-$[PtX_2(SnX_3)_2]^{2-}$ complexes appears as a very low intensity shoulder on the low-energy edge of the UV−visible absorption spectrum. This transition in emission appears as an intense phosphorescence strongly Stokes shifted from the corresponding absorption. Frozen solution emission band maxima are reported for the *cis*-$[PtX_2(SnX_3)_2]^{2-}$ complexes in Table 8 rather than solid state band maxima owing to cation-dependent crystal lattice perturbations that obscure the general trends. These solid state perturbations will be discussed later. The molar absorptivities of all transitions are larger for the bromo complexes than for the analogous chloro complexes, and the phosphorescence lifetime of transition no. 1 is roughly an order of magnitude longer for the chloro complexes than for the corresponding bromo complexes. All the transitions of the $[Pt(SnX_3)_5]^{3-}$ complexes are red-shifted relative to corresponding transitions for the *cis*-$[PtX_2(SnX_3)_2]^{2-}$ complexes. While it is not completely appropriate to compare the transitions of complexes with different molecular symmetry groups, the NMR and X-ray crystallographic data for these species do suggest that the SnX_3^- ligand is a better donor with more s character in the *cis* square planar complexes than in the pentacoordinate complexes.

The molar absorptivity data for the pentacoordinate complexes are puzzling in two aspects: (a) transitions no. 2 and no. 4, based upon the e″- to -a_1' orbital promotion with and without a spin flip, are orbitally forbidden by symmetry, but these transitions have large molar absorptivities; (b) the molar absorptivities of bromo complexes in $[PtX_4]^{2-}$ and *cis*-$[PtX_2(SnX_3)_2]^{2-}$ systems are significantly larger than those of the corresponding chloro complexes, but these trends are reversed for the $[Pt(SnX_3)_5]^{3-}$ complexes. We can rationalize the first of these two puzzles in terms of the stereochemical nonrigidity of the pentacoordinate $[Pt(SnX_3)_5]^{3-}$ complexes at ambient temperature, as the Berry pseudorotation process will relax a selection rule for an otherwise orbitally forbidden transition. The stereochemical nonrigidity argument may also be invoked to explain the second puzzle. As the ^{119}Sn NMR data show, the bulkier $SnBr_3^-$ ligands do not pseudorotate quite as rapidly as do the $SnCl_3^-$ ligands.

Our luminscence data for various $M_3[Pt(SnX_3)_5]$ systems indicate that a small percentage of $M_2[PtX_2(SnX_3)_2]$ may be present as a contaminant in some samples. For example, the

Table 7. Far-Infrared Spectral Data (cm^{-1}) for Nujol Mulls on Polyethylene Thin Films or Polyethylene Disks[a]

compound	ν(SnX)	ν(PtSn)	ν(PtX)
$[Et_4N][SnCl_3]$[b]	280 m, 240 s, 217 s		
$[Ph_4P][SnCl_3]$[c]	292 s, 261 sh, 250 vs		
$[PhCH_2PPh_3][SnCl_3]$[d]	292 vs, 261 sh, 250 sh		
$[Me_4N][SnBr_3]$[e]	202 s, 186 s, 176 s		
$[Et_4N][SnBr_3]$[b]	192 m, 170 s, 148 s, 140 s		
$[Ph_4As][SnBr_3]$[f]	201 s, 183 vs, 176 vs		
$[PhCH_2PPh_3][SnBr_3]$[d]	206, 190 s		
$[PhCH_2PPh_3][PtCl_2(SnCl_3)_2]$[d]	376 m, 338 s	226 m, 202 s	318 vs, 302 s
$[CH_3PPh_3][Pt(SnCl_3)_5]$[d]	376 w, 338 vs	230 w	
$[PhCH_2PPh_2]_3[Pt(SnCl_3)_5]$[d]	376 w, 336 vs	226 w, 210 w	
$[Et_4N]_3[Pt(SnCl_3)_5]$[d]	337 vs	210 s	
$[PhCH_2PPh_3]_2[PtBr_3(SnBr_3)]$[d]	216 vs, 194 s	194 s	216 vs, 258 m, 240 s
$[PhCH_2PPh_3]_2[PtBr_2(SnBr_3)_2]$[d]	220 vs	220 vs	262 m, 254 vs
$[Et_4N]_3[Pt(SnBr_3)_5]$[d]	264 s, 254 s	207 s, 193 s	
$[PhCH_2PPh_3]_3[Pt(SnBr_3)_5]$[d]	246 s, 236 vs	220 s	

[a] Key: vs, very strong; s, strong; m, medium; w, weak; sh, shoulder. [b] Reference 12. See also: Yurchenko, E. N. *J. Mol. Struct.* **1978**, *46*, 319. [c] Reference 26. [d] This work. See also: Yurchenko, E. N.; Antonov, P. G.; Varnek, V. A.; Kornov, V. I.; Shan'ko, A. N.; Kukushkin, Yu. N. *Koord. Khim.* **1976**, *2*, 1632. [e] Reference 13. [f] Wharf, I.; Shriver, D. F. *Inorg. Chem.* **1969**, *8*, 914.

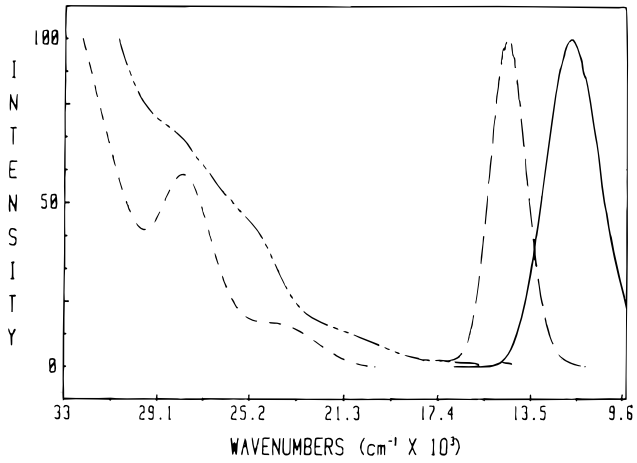

Figure 6. Luminescence and UV−visible absorption spectra of $[CH_3PPh_3]_2[PtCl_2(SnCl_3)_2]$ (- - -; - - -) and $[CH_3PPh_3]_2[PtBr_2(SnBr_3)_2]$ (—; − - - −). The microcrystalline samples were sandwiched between two quartz windows, immersed in a quartz optical dewar filled with liquid nitrogen (77 K) and excited by the pressure-broadened 27 400 cm^{-1} (365 nm) line of a 1000 W Hg/Xe arc lamp to measure luminescence spectra. The room-temperature UV−visible absorption spectra were measured by dissolving known quantities of the microcrystalline samples in Ar-saturated CH_2Cl_2. Pure Ar-saturated CH_2Cl_2 was used as the reference.

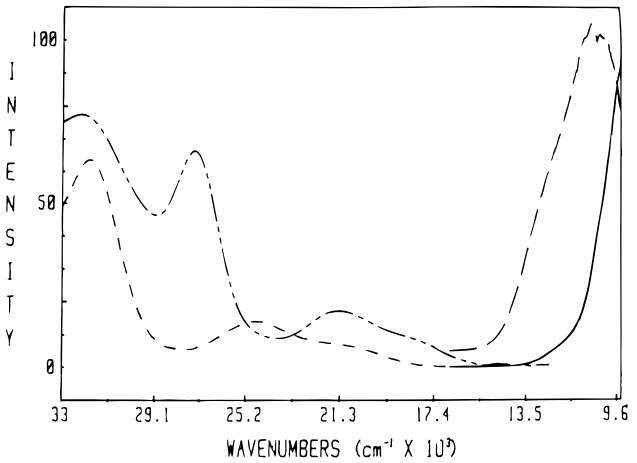

Figure 7. Luminescence and UV−visible absorption spectra of $[CH_3PPh_3]_3[Pt(SnCl_3)_5]$ (- - -; - - -) and $[PhCH_2PPh_3]_3[Pt(SnBr_3)_5]$ (—; − - - −) obtained as in the caption to figure 7.

solid state luminescence spectrum of $[CH_3PPh_3]_3[Pt(SnCl_3)_5]$ exhibits a slight shoulder on the high-energy side of the luminescence maximum that correlates with the luminescence band observed for *cis*-$[PtCl_2(SnCl_3)_2]^{2-}$. In the case of our sample of $[CH_3PPh_3]_3[Pt(SnBr_3)_5]$, we clearly see a small high-energy luminescence band in the solid state that exactly correlates with the luminescence band maximum of *cis*-$[PtBr_2(SnBr_3)_2]^{2-}$. The UV−visible absorption spectrum in solution of this sample is virtually identical to that of $[PhCH_2PPh_3]_3[Pt(SnBr_3)_5]$, which does not show this *cis*- square planar contamination feature. We can explain this by noting that in solution the *cis*-$[PtBr_2(SnBr_3)_2]^{2-}$ and $[Pt(SnBr_3)_5]^{3-}$ species are in equilibrium and the solid samples of the $M_3[Pt(SnBr_3)_5]$ complexes may contain small amounts of the $[PtBr_2(SnBr_3)_2]^{2-}$ species that are a function of the cation. We should note that the luminescence technique is very sensitive such that exceedingly small percentages of contaminants can give rise to measurable spectral features.

There are some problems that arise in the assignment of transition no. 1 for the *cis*-$[PtX_2(SnX_3)_2]^{2-}$ and $[Pt(SnX_3)_5]^{3-}$ species. For both, we have chosen the lowest energy transition in absorption to be the very low absorptivity shoulder on the low-energy edge of the absorption spectra. These shoulders are clearly evident in the spectra of concentrated solutions. Our assignments in Table 8 were guided by the principle of analogy; we preferred to assign transition no. 1 to the low-energy absorption shoulders because many aspects of the *cis*-$[PtX_2(SnX_3)_2]^{2-}$ and $[Pt(SnX_3)_5]^{3-}$ assignments seemed to correlate with the well-established assignments of $[PtX_4]^{2-}$ systems. However, an argument can be made for ascribing these low-energy, low molar absorptivity shoulders to a weak spin−orbit component of the singlet-to-triplet transition no. 1. If this is the case, the main transition is what we have called transition no. 2 in Table 8 and all four other transition assignments are also offest by one transition to higher energy. Certain other compelling analogies emerge among the absorption spectra of $[PtX_4]^{2-}$, *cis*-$[PtX_2(SnX_3)_2]^{2-}$, and $[Pt(SnX_3)_5]^{3-}$ when we accept this offset in our Table 8 assignments, not the least of which is the association of strikingly similar, absorption band shapes and relative band intensities with similar transition assignments. Still another compelling possibility—one that truly lines up the absorption band contours of the square planar and pentacoordinate Pt(II)−SnX_3^- systems with common assignments—is to accept the Table 8 assignments for the *cis*-$[PtX_2(SnX_3)_2]^{2-}$ complexes and invoke the offset for the $[Pt(SnX_3)_5]^{3-}$ complexes. Our difficulty in making choices between these assignments is not without precedent; similar challenges were

Table 8. UV−Visible Absorption Maxima (10^3 cm^{-1}), Molar Absorptivities (in Parentheses; M^{-1} cm^{-1}), and Luminescence Maxima (10^3 cm^{-1}) of Platinum(II) Complexes

	D_{4h} (z) $[PtX_4]^{2-a}$		C_{2V} (y′)[e] *cis*-$[Pt(SnX_3)_2X_2]^{2-}$		D_{3h} (z) $[Pt(SnX_3)_5]^{3-}$	
	Cl	Br	Cl	Br	Cl	Br
1[f]	$^1A_{1g} \rightarrow {}^3E_g$		$^1A_1 \rightarrow {}^3A_2$ or $^3B_2$		$^1A'_1 \rightarrow {}^3E'$	
	17.5-18.0 (6.5-7.9)	16.0-16.2 (9.3-10.2)	20.4 (27)	18.9 (135)	17.4 (270)	15.5 (190)
	$^1A_{1g} \rightarrow {}^3A_{2g}$		$^1A_1 \rightarrow {}^3B_2$ or $^3A_2$		$^1A'_1 \rightarrow {}^3E''$	
2	20.2-20.5 (16.5-18.2)	18.6-18.7 (25.0-26.4)	2.4. (670)	21.7 (1900)	20.9 (4000)	18.3 (2800)
	$^1A_{1g} \rightarrow {}^1A_{2g}$		$^1A_1 \rightarrow {}^1B_2$		$^1A''_1 \rightarrow {}^1E'$	
3	24.8-25.2 (59.6-61.2)	23.2 (126)	27.8 (2670)	25.9 (7900)	24.8 (9400)	21.4 (5107)
	$^1A_{1g} \rightarrow {}^1E_g$		$^1A_1 \rightarrow {}^1B_1$		$^1A'_1 \rightarrow {}^1E''$	
4	29.5-29.9 (66.4-85.1)	26.5-26.9 (187-221)	33.6 (7000)	29.4 (21400)	31.8 (40700)	27.4 (22800)
	$^1A_{1g} \rightarrow {}^1B_{1g}$				charge transfer	
5	37.0 (404-427)	29.7-30.0 (598-640)			38.6 (55100)	32.4 (22800)
	$^1A_{1g} \leftarrow {}^3E_g$		$^1A_1 \leftarrow {}^3A_2$ or $^3B_2$		$^1A'_1 \leftarrow {}^3E'$	
1	12.7[b]	11.7	13.1[c]	11.8[c]	10.6	~97[d]

[a] All $[PtX_4]^{2-}$ Absorption data and assignments from Mason and Gray.[17] [b] Our data and those of Webb and Rossiello[16] coincide. [c] Frozen solution luminescence. [d] Estimated band maximum; actual band maximum is out of the range of our instrument. [e] The *Z* axis is preserved in the same position as D_{4h} to facilitate comparisons between the spectra of D_{4h} and C_{2v} molecules. The principal symmetry axis in this case is chosen to be the *y*′ axis, one of the two axes that bisect Pt−ligand bonds. [f] These numbers are an energy indexing of the electronic transitions.

presented to the researchers who sought to assign the transitions of the $[PtX_4]^{2-}$ complexes.[16−19]

The emissions from the Pt(II)−SnX_3^- complexes are phosphorescences arising from the collapse of the lowest excited triplet state into the singlet ground state. We could not measure lifetimes reliably for the $[Pt(SnX_3)_5]^{3-}$ complexes because their near-infrared luminescences were well out of the range of the optimum sensitivity for the blue-sensitive PMT employed in our lifetime apparatus. Our luminescence lifetime measurements for three *cis*-$[PtX_2(SnX_3)_2]^{2-}$ complexes fall within the range 1−300 μs, typical for phosphorescence transitions in transition metal complexes[27] (Figure 8). The shorter lifetime of the bromo complex compared to those of the two chloro complexes is consistent with the larger molar absorptivity of the bromo complex. The lifetimes exhibit a pronounced temperature dependence characteristic of multiple emission from an excited state (or states) split into closely spaced component states by spin−orbit coupling. In some cases the decay curves are clearly not simple exponential decays, which is also indicative of emission from a multistate excited manifold. The lifetime *vs* temperature curves shown in Figure 8 may be modeled by the Hager−Crosby model.[41] From this model we conclude that, for each of the three cases, the forbidden spin−orbit component of the triplet state must be either the lowest or next to lowest spin−orbit component state in the manifold. Futhermore, if the forbidden state is in fact the next to lowest spin−orbit component, it must lie very near in energy to the lowest allowed spin−orbit state. Since the lifetime is still increasing with decreasing temperature at our low temperature limit (~18−25 K), any decrease in lifetime indicating the presence of an allowed state must occur beneath this low-temperature limit. At the upper bound of our low-temperature limit, 25K, the Boltzmann thermal factor *kT* is 17 cm^{-1}. This factor can be taken as an upper bound to the splitting between a lowest allowed spin−orbit component and a forbidden spin−orbit component.

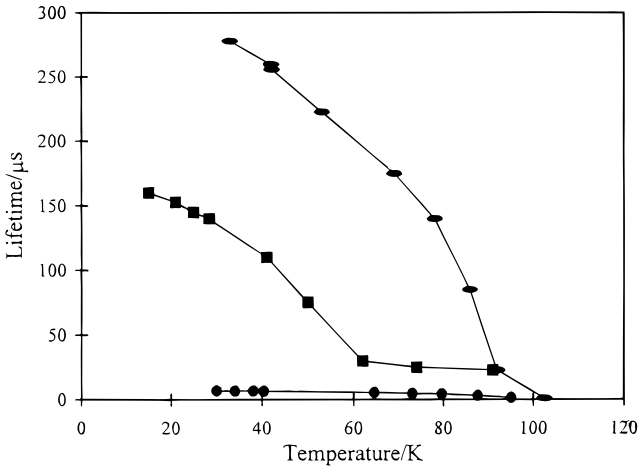

Figure 8. Temperature-dependent luminescence lifetimes of $[CH_3PPh_3]_2[PtCl_2(SnCl_3)_2]$ (oval markers), $[NPr_4]_2[PtCl_2(SnCl_3)_2]$ (square markers), and $[PhCH_2PPh_3][PtBr_2(SnBr_3)_2]$ (round markers). The emission decay signal was measured at the emission maximum and averaged in a digital storage oscilloscope over 60−80 pulses of a nitrogen laser (337 nm excitation). All samples were microcrystalline powders.

If we assume that the phosphorescence of *cis*-$[PtX_2(SnX_3)_2]^{2-}$ arises from a $^3B_2$ excited state (see Table 8), the spin−orbit coupling will split the state into three spin−orbit component states with A, B, and A_2 symmetries. We note that the A_2 state is forbidden in transitions to the A_1 ground state. A Hager−Crosby interpretation of our lifetime data, taken in conjunction with the symmetries of the spin−orbit manifold, implies that the A_2 state must lie at the bottom or near the bottom of the manifold. If we choose our excited state with the alternative $^3A_2$ assignment, the spin−orbit manifold is then composed of A_1, B_1, and B_2 components, each of which is allowed in transitions to the A_1 ground state. Our temperature-dependent lifetime data do not support this assignment from strict symmetry considerations. However, one of the three spin−orbit transition moment integrals could be much smaller than the other two for reasons other than symmetry such as poor Franck−Condon overlap factors.

The band maxima of the 77 K solid state luminescence spectra of the *cis* square planar complexes $[CH_3PPh_3]_2[PtCl_2(SnCl_3)_2]$ (14 440 cm^{-1}), $[PhCH_2PPh_3]_2[PtCl_2(SnCl_3)_2]$ (13 120 cm^{-1}), and $[NPr_4]_2[PtCl_2(SnCl_3)_2]$ (14 190 cm^{-1}) are strongly cation dependent. A similar cation dependence is observed in the solid state luminescence spectra of $[PhCH_2PPh_3]_2[PtBr_2(SnBr_3)_2]$ (12 880 cm^{-1}) and $[CH_3PPh_3]_2[PtBr_2(SnBr_3)_2]$ (12 020 cm^{-1}) at 77 K. However, the UV−visible absorption band shapes and the molar absorptivities of these complexes are virtually identical in solution at ambient temperature. The luminescence band maxima of $[CH_3PPh_3]_2[PtCl_2(SnCl_3)_2]$ (13 110 cm^{-1}), $[PhCH_2PPh_3]_2[PtCl_2(SnCl_3)_2]$ (13 210 cm^{-1}), and $[NPr_4]_2[PtCl_2(SnCl_3)_2]$ (13 280 cm^{-1}) in frozen solution at ~10^{-4} M show only very slight differences. The high-energy 0−0 band edges of the frozen solution luminescence spectra of these three systems virtually coincide at 15 500 cm^{-1}. We postulate that solid state

(41) Hager, G. D.; Crosby, G. A. *J. Am. Chem. Soc.* **1975**, *97*, 7031.

distortions in the crystal lattice are responsible for the solid state luminescence band shifts. Because the solvent used for these frozen solution spectra (CH_2Cl_2) is entirely unsuitable for frozen solution luminescence spectroscopy on a macroscopic scale owing to its tendency to shatter upon freezing and thawing, the novel technique described by Tkachuk and Tolstoi[42] was used to obtain these spectra.

First, the luminescence spectrum of a given solid sample of *cis*-$M_2[PtX_2(SnX_3)_2]$ was measured at 77 K. After warming to room temperature, this solid sample was removed from the low-tempearature sample holder and dissolved in degassed CH_2Cl_2. A glass fiber filter (Reeve Angel, grade 934 AH, size 2.1 cm) was then soaked with this solution. Approximately 3.3 mL and 6.0 mL of degassed CH_2Cl_2 were used for successive dilutions of an initial most concentrated $\sim 10^{-3}$ M solution. Solution concentrations were determined spectrophotometrically. After the dilution, approximately 0.4 mL of solution was used to soak the glass fiber filter. Within 2−3 s after the solution was applied, the well-soaked glass fiber was frozen by immersion in liquid nitrogen at 77 K. The luminescence spectrum of the frozen solution was measured immediately after freezing.

A highly significant and completely unexpected finding of this research is that the frozen solution luminescence band maxima and high-energy 0−0 band edges of the *cis*-$M_2[PtX_2(SnX_3)_2]$ complexes shift as a function of solute concentration. The measured luminescence band maximum of *cis*-$[CH_3PPh_3]_2[PtCl_2(SnCl_3)_2]$ at 77 K in the solid state is 14 440 cm^{-1}, and the 0−0 band edge is 16 300 cm^{-1}. The red-shifted frozen solution luminescence spectra for the first (3.5×10^{-3} M), second (1.1×10^{-3} M), and third (5.1×10^{-4} M) dilutions are virtually superimposable with slight band maxima differences of 13 120, 13 100, and 13 110 cm^{-1}, and the 0−0 band edges all occur at 15 400 cm^{-1}. At room temperature, this complex is very soluble in CH_2Cl_2. The measured band maxima of the luminescence spectra of *cis*-$[PhCH_2PPh_3]_2[PtCl_2(SnCl_3)_2]$ at 77 K in the solid state and in the blue-shifted first (3.3×10^{-3} M), second (1.0×10^{-3} M), and third (4.8×10^{-4} M) dilutions are 12 900, 13 110, 13 110, and 13 210 cm^{-1}, respectively, and the 0−0 band edges all occur at 15 400 cm^{-1}. The *cis*-$[PhCH_2PPh_3]_2[PtCl_2(SnCl_3)_2]$ complex is not as soluble as *cis*-$[CH_3PPh_3]_2[PtCl_2(SnCl_3)_2]$ in CH_2Cl_2. The measured band maxima of the luminesscence spectra of *cis*-$[NPr_4]_2[PtCl_2(SnCl_3)_2]$ at 77 K in the solid state and in frozen CH_2Cl_2 solution for the first (1.3×10^{-3} M), second (3.9×10^{-4} M) and third (1.9×10^{-4} M) dilutions are 14 190, 14 080, 13 320, and 13 280 cm^{-1}, and the corresponding 0−0 band edges appear at 16 100, 15 900, 15 500, and 15 400 cm^{-1}, respectively. The solubilities of *cis*-$[NPr_4]_2[PtCl_2(SnCl_3)_2]$ and *cis*-$[PhCH_2PPh_3]_2[PtCl_2(SnCl_3)_2]$ in CH_2Cl_2 are similar. The luminescence band maxima of *cis*-$[PhCH_2PPh_3]_2[PtBr_2(SnBr_3)_2]$ at 77 K in the solid state and for the first and second dilutions occur at 12 880, 13 250, and 13 190 cm^{-1} with corresponding 0−0 band edges at 16 000, 15 900, and 15 100 cm^{-1}. The measured luminescence band maxima of *cis*-$[CH_3PPh_3]_2[PtBr_2(SnBr_3)_2]$ at 77 K in the solid state and in poly(methyl methacrylate) are 12 020 and 12 050 cm^{-1}. The solubility of *cis*-$[PhCH_2PPh_3]_2[PtBr_2(SnBr_3)_2]$ in CH_2Cl_2 is very low at room temperature; reliable concentration data for this compound could not be obtained spectrophotometrically.

Trends in the solvent shift data are, at first glance, bewildering. Progressive dilutions (from solid state to lowest concentration in solution) of the complexes *cis*-$[PhCH_2PPh_3]_2[PtX_2(SnX_3)_2]$ (X = Cl, Br) and *cis*-$[CH_3PPh_3]_2[PtBr_2(SnBr_3)_2]$ give small progressive luminescence blue-shifts at 77 K. The complexes *cis*-$[CH_3PPh_3]_2[PtCl_2(SnCl_3)_2]$ and *cis*-$[NPr_4]_2[PtCl_2(SnCl_3)_2]$ exhibit large luminescence red shifts with progressive dilutions. The luminescence band of *cis*-$[CH_3PPh_3]_2[PtCl_2(SnCl_3)_2]$ strongly red-shifts upon the first dilution, but further dilutions produce no changes in the luminescence spectra. For *cis*-$[NPr_4]_2[PtCl_2(SnCl_3)_2]$ a progressive luminescence red shift is observed with successive dilutions of the sample.

The key to understanding these trends lies in considering distortions of the square planar unit. A severe in-plane angular distortion of the square planar unit is evident from the solid state X-ray crystallographic data for *cis*-$[PhCH_2PPh_3]_2[PtCl_2(SnCl_3)_2]$: Sn−Pt−Sn = 111.48(3)°, Cl−Pt−Cl = 101.32(8)°. A smaller planar distortion is observed for *cis*-$[CH_3PPh_3]_2[PtBr_2(SnBr_3)_2]$: Sn−Pt−Sn = 96.1(1)° but Sn(3)−Pt(2)−Sn(3a) = 111.8 (1)° and Br(1)−Pt(1)−Br(2) = 90.6(1)° but Br(3)−Pt(2)−Br(4) = 99.2 (1)°. From these crystallographic data it is reasonable to assume that the "square planar" units of the other complexes for which X-ray data are not available are also distorted to similar extents in their solid state crystalline environments. Moreover, we expect that both the nature and extent of the distortions could be cation dependent. It is also reasonable to assume that these distortions may change when the compounds are dissolved in solution and crystal packing effects are replaced by solvation effects. The final geometry in solution should be one that minimizes the ground state energy of the square planar unit in solution. The adjustment of the geometry of the square planar unit in solution will also change the HOMO to LUMO energy gap compared to that in the solid state. We can reasonably expect to encounter cation−complex anion pairs for which this gap increases (luminescence blue shift) and other cation−complex anion pairs for which this gap decreases (luminescence red shift) on going from the solid state into solution.

If it is assumed that for all the complexes the distortions are confined to the plane, we can readily relate planar angular distortions to changes in the HOMO-to-LUMO = d_{xy} to $d_{x^2-y^2}$ energy gap. Note that we adopt the HOMO-to-LUMO $a_1(d_{xy})$-to-$b_2(d_{x^2-y^2})$ orbital promotion assignment to give a $^3B_2$ excited state as supported by our temperature-dependent lifetime data. In a perfect 90° square planar complex, the lobes of the Pt d_{xy} orbital fall exactly between the ligands and the Pt $d_{x^2-y^2}$ orbital lobes exactly coincide with the metal−ligand axes, here assumed by common convention to be the *X* and *Y* axes. Simple ligand field and AOM arguments tell us that the $d_{x^2-y^2}$ orbital energy will lie above that of the d_{xy} orbital. As the ligands move away from the *X* and *Y* axes in the *XY* plane, the $d_{x^2-y^2}$ orbital becomes stabilized and the d_{xy} orbital is destabilized. This will result in a decreased energy gap and a red shift in the luminescence. It is interesting to note that the *cis*-$[PtCl_2(SnCl_3)_2]^{2-}$ anion with the two smallest cations $[CH_3PPh_3]^+$ and $[NPr_4]^+$ exhibits large solution luminescence red shifts with reference to the solid state luminscence band positions. For the larger complex anion, *cis*-$[PtBr_2(SnBr_3)_2]^{2-}$, or for either the bromo or chloro complex with large cations, the crystal packing forces are less constraining and the difference in the HOMO-to-LUMO energy gap in solution *vs* that in the solid state is much smaller.

We are left to explain the progressive luminescence band shift that is observed for some of the complexes with increasing dilution. The combined effects of solvent shrinkage (∼20−30% at 77 K *vs* 300 K) and thin film surface phenomena are estimated to increase the effective concentrations of the complexes on the frozen glass filter by roughly 1 order of magnitude. We postulate that the surface effects and the cryogenic effects operate cooperatively according to the following model. When a droplet of room-temperature solution is applied to the porous glass filter, most of the CH_2Cl_2 solvent

(42) Tkachuk, A. M.; Tolstoi, N. A. *Opt. Spektrosk.* **1965**, *20*, 1030.

molecules not in the solvation spheres of the cations and anions will be drawn out onto the glass surface to form a thin solvent film. The solvation spheres will also experience some solvent molecule depletion and contract. These effects will further increase the effective concentrations. Cooling to cryogenic temperatures reduces solvent volume even more, further increasing the concentration. Within this concentration regime, progressive band shifts based upon concentration-dependent aggregation seem reasonable.

Acknowledgment. It is a pleasure to acknowledge the assistance of Casey Joseph in measuring electronic absorption spectra and Durwin Striplin, M. Inga Kenney, and Kyle Hamor in writing the luminescence data acquisition/plotting software. We are grateful to the donors of the Petroleum Research Fund, Administered by the American Chemical Society, and to the Llano Estacado Center for Advanced Professional Studies and Research for financial support, to Johnson Mathey Aesar/Alfa for a generous loan of K_2PtCl_4, to the National Science Foundation (Grant CHE-9214294) for funds to purchase the NMR spectrometer, to the Hewlett-Packard Foundation for the donation of the diode array UV−visible spectrophotometer, and to the Air Force office of Scientific Research for funds to purchase the digital storage oscilloscope.

Supporting Information Available: Figure S-1, showing the 186.36 MHz ^{119}Sn NMR spectra of $[PhCH_2PPh_3]_2[PtBr_3(SnBr_3)]$ and $[PhCH_2PPh_3]_2[PtBr_2(SnBr_3)_2]$ in acetone-d_6 at 298 K, Figure S-2, showing the UV−visible absorption spectrum of $[NPr_4]_2[PtCl_2(SnCl_3)_2]$, and for the crystal structures, listings of crystal and refinement data, positional parameters for non-H atoms (Tables 2 and 3), bond distances and angles, H atom coordinates, and thermal parameters (20 pages). Ordering information is given on any current masthead page.

IC9507878